Effect of Hydrophobicity and Charge Separation on the Antifouling Properties of Surface Tethered Zwitterionic Peptides

Chuanxi Li [a, b, c, e], *Minglun Li* [b], *Wei Qi* [b, c], *Rongxin Su* [a, c, d, *], *Jing Yu* [b, *]

[a] State Key Laboratory of Chemical Engineering, Tianjin Key Laboratory of Membrane Science and Desalination Technology, School of Chemical Engineering and Technology, Tianjin University, Tianjin 300072, PR China

[b] School of Materials Science and Engineering, Nanyang Technological University, Singapore 639798, Singapore

[c] Collaborative Innovation Center of Chemical Science and Engineering (Tianjin), Tianjin 300072, PR China

[d] School of Marine Science and Technology, Tianjin University, Tianjin 300072, PR China

[e] Petrochemical Research Institute, PetroChina, Beijing 102206, PR China

KEYWORDS: zwitterionic, peptide, antifouling, charge separation, hydrophilicity

Abstract

Zwitterionic peptides emerge as a class of highly effective antifouling materials in a wide range of applications such as biosensor, biomedical devices, and implants. We incorporated neutral amino acid spacers with different hydrophobicities, including serine (Ser), glycine (Gly), and leucine (Leu), into zwitterionic peptides with KE repeating units and investigated the structure and antifouling performance of the zwitterionic peptide brushes using surface plasma resonance (SPR), surface force apparatus (SFA), and all atomistic molecular dynamics (MD) simulation techniques. Our results demonstrate that the hydrophilicity of neutral spacers alters the structure and antifouling performance of the peptide-modified surface. Hydrophilic Ser inserted peptides reduced the interaction between the peptide monolayer and protein foulants while hydrophobic Leu significantly increased the protein adhesion. SFA force measurements shows that the presence of more spacers would increase the adhesion between the peptide monolayer and the modeling foulant lysozyme, especially for the hydrophobic spacers. MD simulations reveal that hydrophilic Ser spacers retain the hydrophilicity of the peptide monolayer and improve the antifouling performance, and Gly spacers give rise to more inter-chain crosslinks. Leu spacers result in a more hydrophobic peptide monolayer which lead to dehydration of the peptide monolayer and reduces the antifouling performances.

Introduction

Fouling of biomolecules and microorganisms is a great challenge in many applications, such as medical devices, drug delivery and purification systems.[1-3] The biofilm-infected medical devices cause more than 45% of hospital-contracted infections and about 10% of hospital patients suffer infection from clinical implants.[4] Surface tethered hydrophilic polymers such as polyethylene glycol (PEG) and their analogs have been suggested as effective antifouling candidates.[5-9] However, PEG is subject to degradation, and the biomedical applications of PEG are limited by its immunogenicity.[10-12] It is essential to develop novel antifouling materials for more practical applications.[13, 14]

Owning good biocompatibility and excellent antifouling performance, zwitterionic polymers have received great attention. With equal positive and negative charges in the same functional unit, zwitterionic polymers such as poly(carboxybetaine methacrylate) (PCBMA),[15, 16] poly(sulfobetaine methacrylate) (PSBMA),[17, 18] and poly(2-methacryloyloxyethyl phosphorylcholine) (PMPC)[19, 20] have strong hydration arising from the electrostatic attraction between the charged residues and water molecules. The hydration layer repels the foulants approaching to the zwitterionic polymers, and the charge neutrality of the polymer diminishes the electrostatic attractions between the foulants and the polymers. The zwitterionic nature makes such polymers a promising class of material for a wide range of biomedical applications.[21]

Zwitterionic peptides consist of alternating positively and negatively charged amino acid residues.[22] Comparing with the zwitterionic polymers, zwitterionic peptides are inherently

biodegradable. Additionally, we can readily tune the compositions and chain length of the peptides through controlling the peptide sequences,[23, 24] and a variety of natural and synthetic amino acids can be utilized. These advantages make zwitterionic peptides very attractive in a wide range of applications, such as drug delivery,[25, 26] medical implants,[27] and biosensors[28, 29]. The structure and antifouling properties of zwitterionic peptides have been investigated by experiments and molecular dynamic (MD) simulation. Jiang's group found that a linker consisting of 4-proline (PPPP) increased the modification density of the self-assembled monolayers (SAMs) and improved the antifouling performance of the coated surface.[30] They also studied the impact of monovalent salts to the antifouling performance of lysine-glutamic acid (KE) zwitterionic peptides[31] and reported that the adsorption of lysozyme to a zwitterionic brush increases as the ionic strength decreases. Recently, our group systematically investigated the antifouling performance of a series of zwitterionic peptides with different chain lengths and charge distributions. Divalent ions can increase the adsorption of BSA to the zwitterionic peptides, especially for peptides with block charges.[32]

Inserting different amino acids into zwitterionic peptides can disrupt the electrostatic interactions between the charged amino acid residues, altering the structure of surface tethered peptide monolayers. Zhang *et. al.* discovered that an Alanine spaced zwitterionic peptide $(AEAEAKAK)_2$ can form stable macroscopic membrane in solution.[33] The combination of hydrophobic interactions between alanine residues and electrostatic interactions between charged residues promotes the formation of β-sheets between the peptides, resulting macroscopic aggregates in solution. Jiang's group reported that separating the superhydrophilic

$(EK)_{15}$ with glycine (G) residues promotes disordered conformations of the peptides at physiologically relevant temperature[34], which adds flexibility and improves the hydration of the peptides. The rich choices of the amino acids that can be included in the zwitterionic peptide sequences pose steep challenges, as cautions must be taken to avoid unwanted interactions between the peptide chains as well as between the peptides and other biological molecules.

Despite of previous efforts, how including different amino acids to the sequence of zwitterionic peptides affects the structure and properties of the peptides remains poorly understood. In this work, we incorporated three neutral amino acid spacers with different hydrophobicities, including serine (S), glycine (G), and leucine (L), into zwitterionic peptides with KE repeating units. The effect of the neutral amino acid spacers to the structure and antifouling properties of the surface tethered zwitterionic peptides were studied with surface plasma resonance (SPR), atomic force microscopy (AFM), surface force apparatus (SFA), and bacteria adhesion assay. All-atom molecular dynamic simulations were employed to elucidate the structures of the zwitterionic peptide monolayers. Our results demonstrate that separating zwitterionic units by hydrophilic amino acid instead of glycine or hydrophobic amino acid improve the antifouling performance of the coated surface.

Results and Discussion

Effect of charge separation on modification

To study the effect of spacer between charges in the zwitterionic peptides, we separated the positively charged lysine (K) and negatively charged glutamic acid (E) residues with three

neutral amino acid with different hydrophobicities: EK by serine (S), glycine (G), and leucine (L). Six different amino acids with KXKE or KX_2KE_2 repeating units were designed, where X = S, G, or L. A 4-proline (CPPPP) unit was included to the N terminus of each peptide to facilitate the assembly of the peptides on gold surfaces.[30] We grafted the zwitterionic peptides to the gold surface by using the well-established thiol-gold chemistry[35] (Figure S2). For consistency, a glutamic acid was used as the ending group at the C terminus for all the peptides (Scheme1).

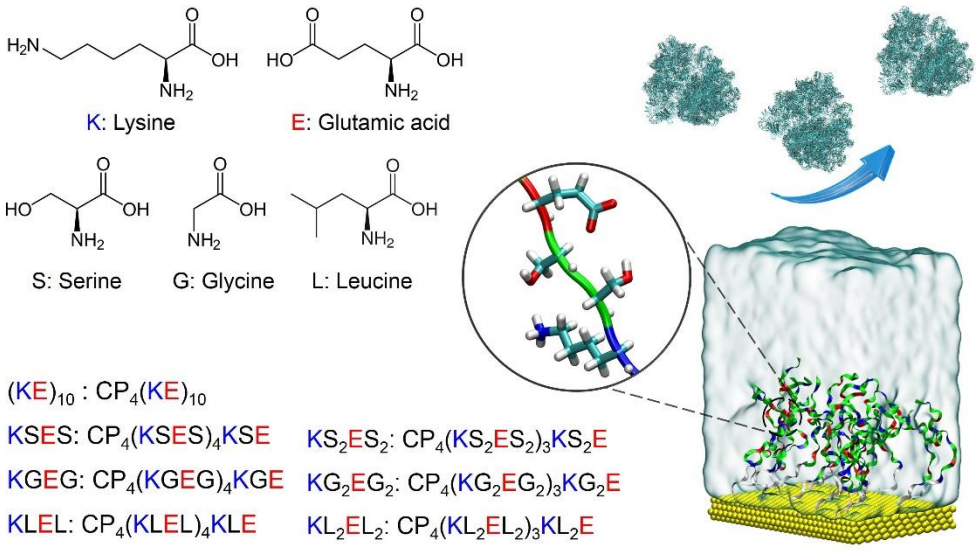

Scheme 1. Schematic diagram and sequences of the zwitterionic peptides. Chains represent the modified peptides and background represents the water molecules. The molecules on the top are the protein foulants.

We first studied the surface assembly behaviors of the zwitterionic peptides on the gold surface in real time (Figure 1a) by the surface plasma resonance (SPR) technique. The peptide was grafted to a gold substrate by flowing a solution containing 0.015 mM peptide through the

SPR chamber with a 5 μL/min flow rate for 40 min. The final grafting density for peptides KSES, KGEG, and KLEL inserted peptides were 0.061, 0.077, and 0.059 nmol/cm^2, respectively, correspond to 0.37, 0.47, and 0.36 chain/nm^2. Due to the high flexibility of glycine, peptides KGEG has the highest grafting density. For the peptides with the same amino acid spacer, the number of spacers between charged amino acids does not significantly affect the grafting density of the peptides, e.g., Peptides KXKE and KX_2KE_2 have almost identical grafting densities (Figure 1b).

The hydrophilicity of the zwitterionic peptide monolayers significantly changes with the type and number of the neutral spacer in the peptide sequences. The contact angle of a gold substrate was 80.8±7.2 °, and the contact angle of the substrate decreased to 14.5 - 50.1 ° after the peptide modification (Figure 1c). The contact angle of peptide KSES (13.2 ± 1.7 °) was almost identical to that of peptide $(KE)_{10}$ (14.5 ± 1.8 °). Replacing the Ser with Gly slightly increased the contact angle of the peptide monolayer to 15.7 ± 2.7 °. Further replaced the Gly with more hydrophobic Leu significantly increased the contact angle to 47.7 ± 3.2 °, indicating the effect of the hydrophobic spacer to the overall hydration of the peptide monolayers. For all three spacers tested, increasing the number of spacers between the charged amino acids from 1 to 2 increases the contact angle of the peptide monolayers. As we increase the number of spaces in the peptide sequence, the number of changed amino acids decreases, which increases the overall hydrophobicity of the peptides. Our contact angle measurements show that both the hydrophobicity of the spacer amino acids and the number of the spacers can significantly change the hydrophobicity of the surface tethered zwitterionic peptide monolayers, which can

affect their antifouling properties.

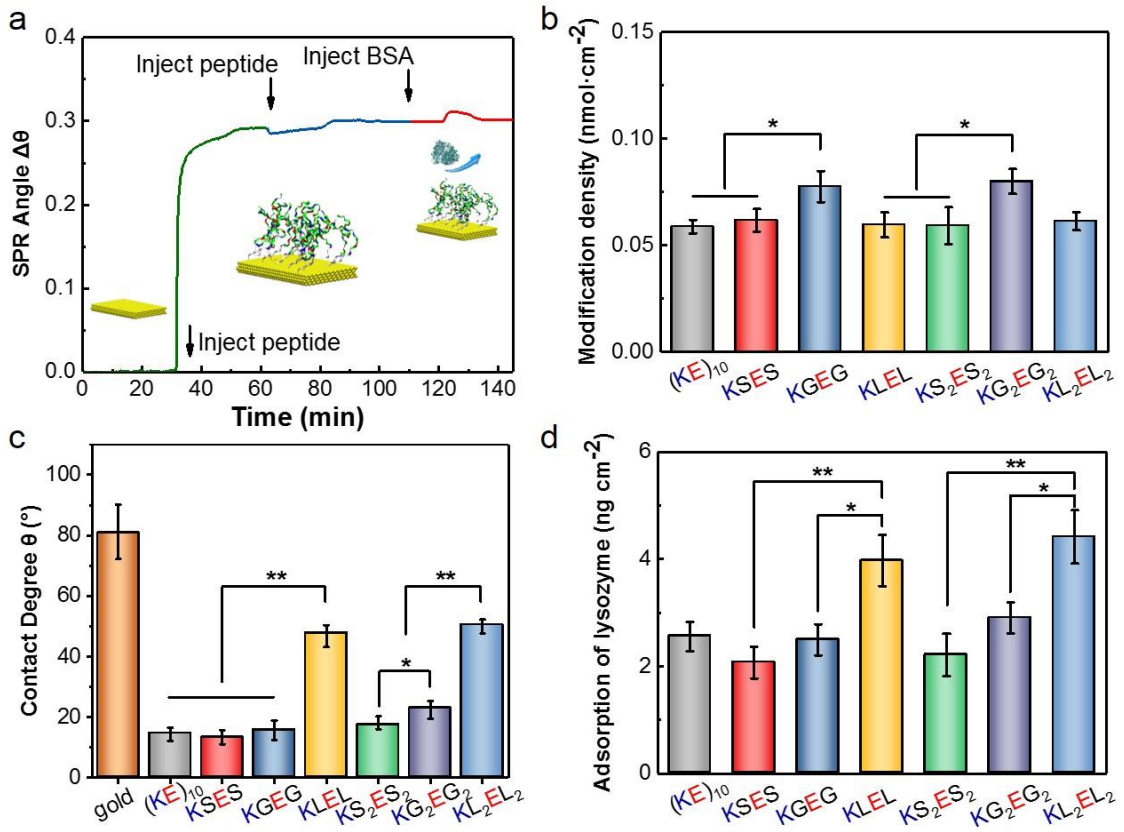

Figure 1. The modification and antifouling properties of different zwitterionic peptide monolayers. (a) An example of the SPR curve of the modification and anti-adsorption experiment; (b) the modification density of different peptides on gold substrates; (c) the contact angle of water on different peptide-modified gold surfaces; (d) the adsorption of lysozyme on the gold surfaces modified with different peptides. (**) $p<0.01$, (*) $p<0.05$.

Using a SPR, we also systematically investigated the antifouling properties of the hybridized zwitterionic peptides. Positively charged lysozyme and negatively charged bovine album serum (BSA) were used as model foulants. The hydration of zwitterionic peptides is critical to their antifouling performacne.[32] Compared with the bare gold, the presence of zwitterionic peptide monolayers dramatically reducing the fouling of lysozyme and BSA

(Figure S3a). All the designed zwitterionic peptides show very low lysozyme adsorption (< 4.5 ng/cm^2). Gly spacers showed the minimum effect on the lysozyme adsorption as peptides KGEG showed almost identical lysozyme adsorption as the control peptide $(KE)_{10}$. Surprisingly, peptides KSES showed slightly better antifouling performance than the control sequence $(KE)_{10}$. The lysozyme adsorptions were 2.5 ± 0.2 and 2.1 ± 0.2 ng/cm^2 for peptides $(KE)_{10}$ and KSES, respectively. We attribute this to the hydrophilic nature of the Ser residues. On the contrary, the insertion of hydrophobic Leu spacer increases the lysozyme adsorption to 3.9 ± 0.4 ng/cm^2. A similar trend was observed when using BSA as the foulant (Figure S3b). For all three amino acid spacers, the lysozyme adsorption increased as increasing the number of spacers between Lys and Glu from 1 to 2 (Figure 1d). This is likely due to the smaller number of charged residues in the peptides KS_2ES_2, KG_2EG_2, and KL_2EL_2. The SPR results clearly demonstrate that the hydrophobicity of the spacers significantly affects the antifouling performance of the peptide-modified surface.

The morphology and surface force of zwitterionic peptide monolayers.

In order to further understand the effect of different spacers on the zwitterionic peptide, we investigated the morphology of different zwitterionic peptide monolayers in PBS buffer using atomic force microscopy (AFM) with ScanAsyst mode. The AFM images of the peptide monolayers indicate the all peptides are uniformly tethered to the gold surfaces (Figure 2), with the mean squared roughness of between 0.5 - 0.8 nm (Table S6).

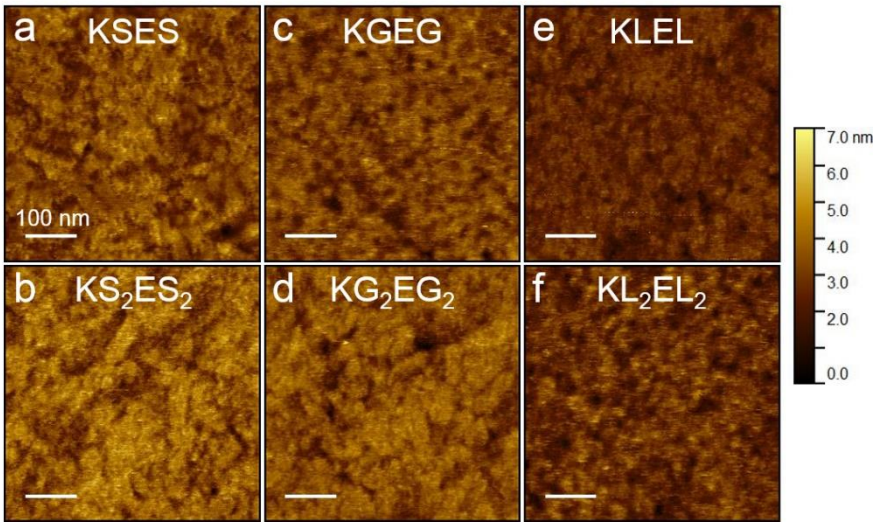

Figure 2. AFM morphological images the surface modified with (a) KSEGE, (b) KS_2ES_2, (c) KGEGE, (d) KG_2EG_2, (e) KLELE, (f) KL_2EL_2 in PBS buffer. The scale bar is 100 nm.

To explore the antifouling mechanism of the peptide monolayers, we used the surface force apparatus (SFA) technique to measure the interactions between a surface tethered monolayer and a mica surface modified by lysozyme. Since BSA is negatively charged in solution, it does not adsorb on negatively charged mica surface. We therefore chose positively charged lysozyme as the model foulant. The force between a peptide monolayer and a bare mica surface was first measured as a function of the separation distance (D) between the surfaces (Figure 3 and Figure S5). The thickness of the peptide layers was estimated by the hard wall separation distance measured in the force-distance profile between the peptide monolayer and the bare mica surface. SFA measurements showed that for peptides KSES, KGEG, and KLEL, the thicknesses of the surface tethered peptide monolayers were all ~ 5 nm. However, the force-distance profiles of the three peptide monolayers against a bare mica surface were very different. Perfect reversible force-distance curves were measured upon

approaching and separating two surfaces for peptide KSES, and the interaction was purely repulsive. The repulsion measured for the KSES monolayer started from 11 nm. In contrast, monolayers formed by peptides KGEG and KLEL showed very different force-distance profiles: the repulsion only showed up at a distance of ~ 7 nm during the approaching and an adhesion force was measured during the separation. The adhesion force *F/R* measured was -0.11 and - 0.52 mN/m for the KGEG and KLEL peptide monolayers, respectively. The thickness of peptide monolayers KS_2ES_2, KG_2EG_2, and KL_2EL_2 slightly increased to 6.8, 5.5, and 6.3 nm, respectively. Interestingly, KG_2EG_2 monolayer showed the smallest thickness among the three peptides, likely due to flexibility of the Gly residues, while the KS_2ES_2 monolayer had the largest thickness due to the strong hydration of the peptide chains. The force-distance profiles of the three peptides showed the same trends to the force profiles of KSES, KGEG, and KLEL, but the adhesion forces measured for peptides KG_2EG_2 and KL_2EL_2 were stronger than these of peptides KGEG, and KLEL. The difference in the SFA force curves from the peptides with Ser, Gly, and Leu spacers are caused by the difference in the hydrophobicity of the three spacers. Due to the hydrophilic nature of Ser, peptide KSES is more hydrophilic, leading to strong hydration of the peptide monolayer and therefore a purely repulsive force-distance profile. In contrast, the hydrophobic Gly and Leu residues can significantly perturb the hydration of the zwitterionic peptide, which can facilitate the hydrogen binding between the peptide monolayer and the mica surface, resulting in adhesion between two surfaces[36].

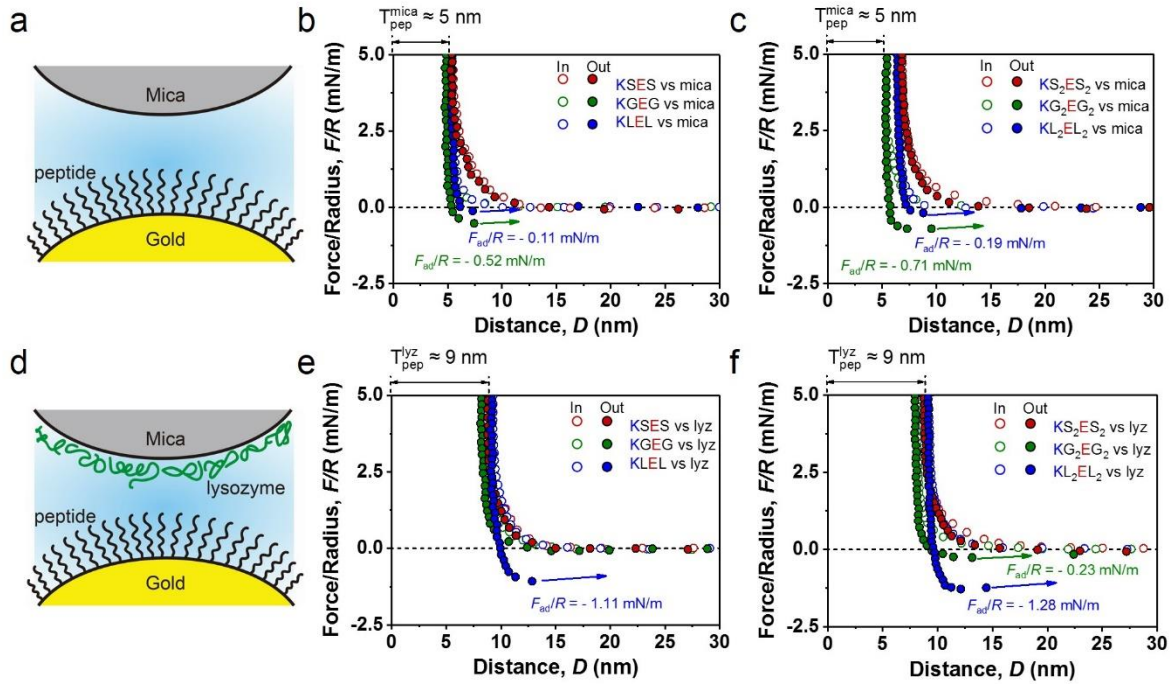

Figure 3. SFA measurements on peptide monolayers. Illustration of the SFA experimental system with (a) bare mica and (d) lysozyme-coated mica surfaces. SFA force curves between a bare mica and the gold surface modified by (b) peptides KSES, KGEG, and KLEL as well as by (c) peptides KS_2ES_2, KG_2EG_2, and KL_2EL_2. SFA force curves between a lysozyme layer and the gold surface modified by (e) peptides KSES, KGEG, and KLEL as well as by (f) peptides KS_2ES_2, KG_2EG_2, and KL_2EL_2. The adhesive force F normalized by the curvature of the surfaces (R) was determined at the point of surface detachment (indicated by an arrow).

The interactions between the peptide monolayers and a thin lysozyme protein layer were then measured using an SFA. Lysozyme and bare gold surface have strong adhesive interactions (F/R = - 1.71 mN/m). (Figure S5). After coating the gold surface with different zwitterionic peptides, the measured adhesive force decreased significantly. The force curves measured from peptides KSES, KGEG, and KLEL showed almost identical approaching with a repulsion arising at a distance of 15 nm and a hard wall of 9 nm. As the thickness of the peptide monolayer

was about 5 nm, this indicates that the thickness of the lysozyme monolayer was around 4 nm. Upon separation, no adhesion was measured between a peptide KSES or KGEG monolayer against a lysozyme monolayer, whereas an adhesion of - 1.11 mN/m was measured for peptide KLSL. The force-distance profiles measured with peptides KS_2ES_2, KG_2EG_2, and KL_2EL_2 show similar trends to peptides KSES, KGEG, and KLEL. However, stronger adhesion was measured during the separation. The force-distance profile showed that there was no adhesion between the lysozyme layer and a KGEG monolayer, but a small adhesion force (- 0.23 mN/m) was measured with a KG_2EG_2 monolayer. Similarly, the KL_2EL_2 monolayer showed stronger the adhesion force (- 1.28 mN/m) on lysozyme in comparison to the KLEL monolayer.

Our SFA force measurements between the zwitterionic peptide monolayers and a lysozyme layer agree well with the SPR measurements on the lysozyme adsorption on the spacer inserted peptide monolayers. The peptides with hydrophilic Ser spacers showed no adhesion force against a lysozyme monolayer in the SFA measurements and the lowest lysozyme adsorption in the SPR tests, whereas the SFA force curves from the peptides with hydrophobic Leu spacers showed the strongest adhesion force against a lysozyme monolayer, resulting in strong lysozyme adsorption. Depending on the hydrophobicity of the spacers, the insertion of the neutral spacer in the zwitterionic peptide sequence can strongly alter the interaction between the zwitterionic peptides and the protein foulants in solution and affect the antifouling properties of the peptide monolayers.

Anti-bacterial performance

We tested the anti-bacteria performance of our spacer inserted zwitterionic peptide monolayers using the green fluorescent protein expressing E. coli. The adsorption of the bacteria on surface was monitored as a function of the averaged fluorescence signals from the surface. The representative fluorescent micrographs indicate significant adhesion of E. coli on bare gold surface after one day of incubation (Figure 4). Upon coating the gold surfaces, the fluorescence intensity from the surface adhered bacteria decreased by 92.1±0.7 %, 97.4±0.2 %, 92.4±0.6 %, and 88.8±1.5 % for peptides $(KE)_{10}$, KSES, KGEG, and KLEL-modified surfaces, respectively. The anti-bacteria performance of the neutral spacer inserted peptides again confirms that the addition of hydrophilic Ser residues into the zwitterionic peptide sequence can slightly improve the anti-bacteria performance of surface tethered zwitterionic KE peptides, whereas the insertion of hydrophobic Leu residues increases the adhesion of E. coil on zwitterionic peptide-modified gold surfaces (Figure 4).

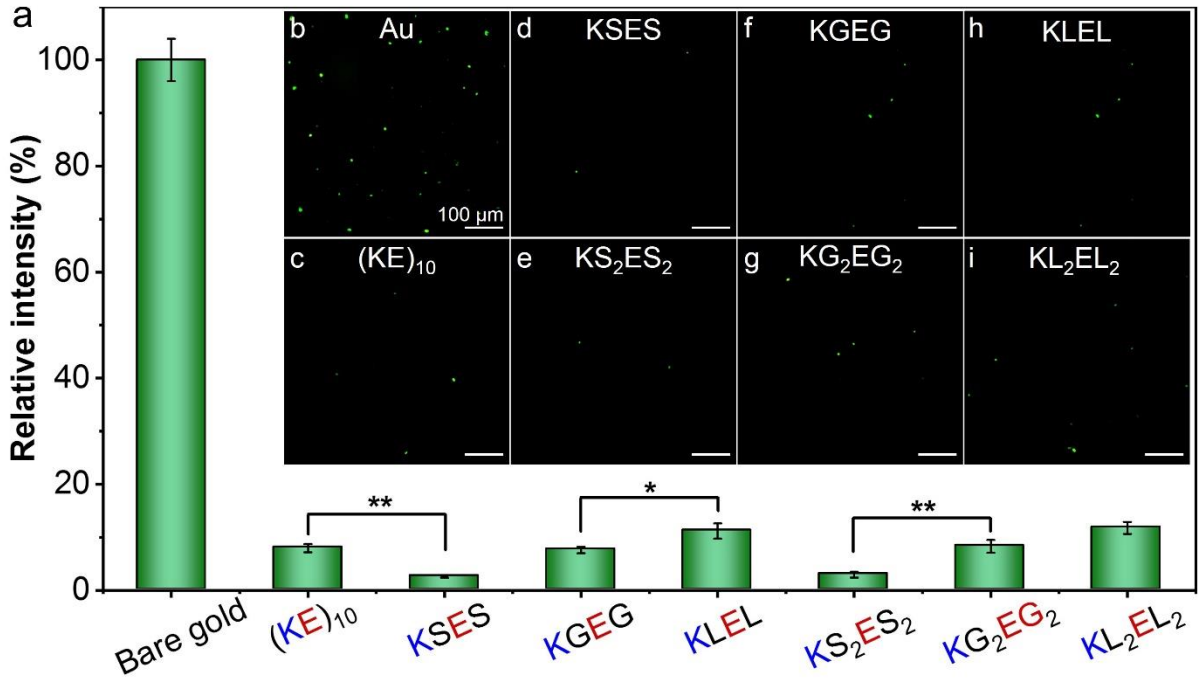

Figure 4. (a) The fluoresces intensity and images of green fluorescent protein (GFP) on the (b) bare gold or the gold surface modified by (c) $(KE)_{10}$, (d) KSESE, (e) KS_2ES_2, (f) KGEGE, (g) KG_2EG_2, (h) KLELE, (i) KL_2EL_2. The scale bar is 100 μm. (**) $p<0.01$, (*) $p<0.05$.

Molecular dynamic simulation

We used all-atom molecular dynamics (MD) simulations to further investigate the mechanisms of the antifouling properties of the zwitterionic peptide with neutral amino acid spacers at the molecular level. Using GROMACS 5.1.4,[37] three peptides, KS_2ES_2, KG_2EG_2, and KL_2EL_2 were simulated, and the grafting density of each peptide was chosen according to the SPR measurements. Figure 5a-c show the snapshots of the peptide monolayers on gold surfaces after reaching equilibrium. The snapshots reveal while all three peptide monolayers exhibit polymer brush like structures at the experimental grafting density. Peptide KS_2ES_2 monolayer has the highest height whereas the KG_2EG_2 monolayer shows the lowest height. In last equilibrated 10 ns, the time-averaged atom density distributions along the z-axis for the three peptide monolayers also show the same trend (Figure 5d). The atom density distributions along the z-axis of all three peptides exhibit a peaked distribution with the maximum located at about the middle of the peptide monolayer. The end of the atom density distribution of the KS_2ES_2 monolayer reaches 7 nm while that of the KG_2EG_2 monolayer is only slightly over 5 nm. The thickness of the peptide monolayers obtained from MD simulations agree surprisingly well with the thickness of the same peptide monolayers measured with the SFA (Figure 3).

The MD simulations provide critical insights on the structures of the surface tethered

zwitterionic peptide monolayers. Our previous studies have shown that the alternating charges of the Lys-Glu repeating units in zwitterionic peptides can lead to interchain electrostatic interactions between surface tethered peptide brushes. [32] The insertion of neutral amino acid spacers reduces the charge density of the zwitterionic peptides and therefore can significantly affect the electrostatic interactions between the charged groups. Due to the flexibility of Gly, the KG_2EG_2 peptides tend to have stronger electrostatic interactions with the neighboring chains, resulting in more interchain crosslinks and a more compacted monolayer. In comparison, the Ser and Leu spacers lead to more extended peptide chains on the gold surface.

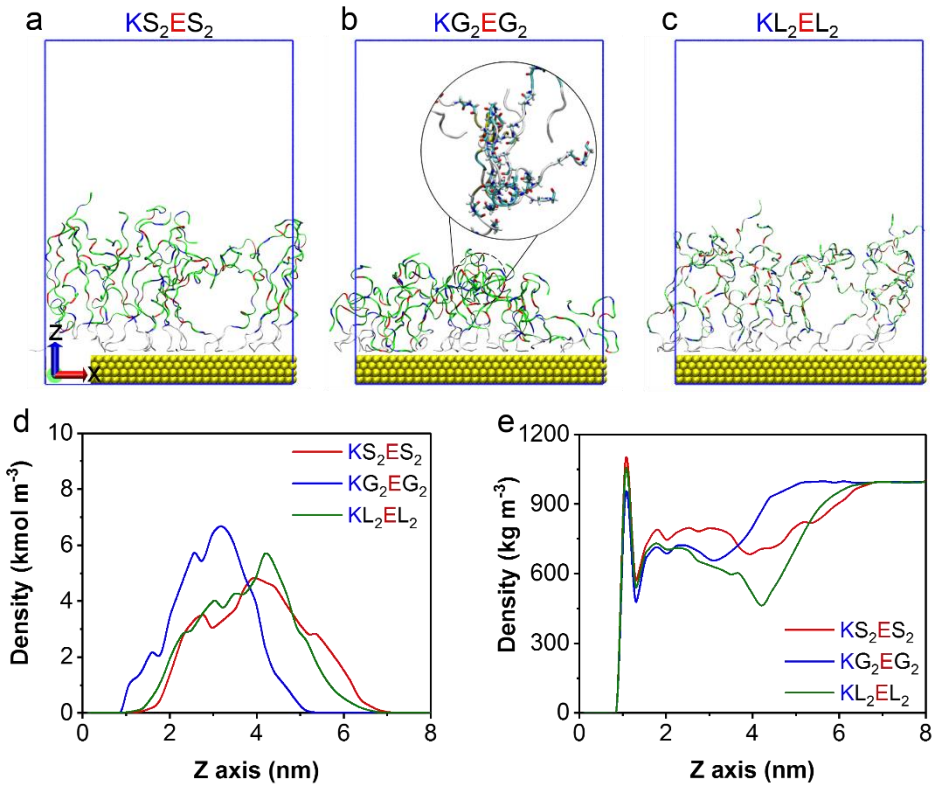

Figure 5. The molecular dynamic simulation snapshot of (a) KS_2ES_2, (b) KG_2EG_2, (c) KL_2EL_2. The density distributions of the (d) peptide layers and (e) water in different systems. The gold surface is from 0 to 0.85 nm along the z-axis.

Hydration is essential to the structure and properties of zwitterionic peptides.[38] To investigate the differences of water distributions in different peptide monolayers, we plotted the time averaged density distribution of water along the z-axis for different peptide monolayers. The distribution of water molecules is related to the hydrophilicity of spacers (Figure 5e). Due to the presence of the peptides, the density of water in the peptide brush is smaller than the bulk phase, and the density of water gradually increases at the interface of the peptide brush. For KS_2ES_2 and KL_2EL_2, the density distribution of water increase at around 4.2 and 3.9 nm, respectively, and become stable after ~7.3 nm. While the density distribution of water of KG_2EG_2 increases at around 3.2 nm and become stable after 5.5 nm due to the smaller thickness of the KG_2EG_2 monolayer. Moreover, the density of water in the KL_2EL_2 monolayer is smaller than that of KS_2ES_2 and KG_2EG_2, indicating there are less water molecules around KL_2EL_2 peptides. This is due to the hydrophobic Leu residues, which disrupt the hydration layer of the zwitterionic peptides. In comparison, the density of water in the KS_2ES_2 monolayer is larger than that in the other two peptides, indicative of a more hydrated peptide monolayer due to the presence of the hydrophilic Ser residues.

Conclusions

We studied the effect of three neutral amino acid spacers, Ser, Gly, and Leu, to the structure and antifouling properties of zwitterionic peptide monolayers. Our results demonstrate that the hydrophobicity of the neutral amino acids in the zwitterionic peptide sequences can strongly alter the hydrophobicity of the surface tethered zwitterionic peptide

brushes. With all the peptides tested, the Ser inserted peptides showed the best antifouling performance while the Leu incorporated peptides performed poorly. The SFA force measurements reveal that inserting hydrophobic Leu residues into the zwitterionic peptide chains increase the adhesion between the peptides and proteins in solution, which explains the poor antifouling performance of Leu incorporated zwitterionic peptides. MD simulations reveal that including hydrophilic Ser residues in the sequence of zwitterionic peptides preserves the hydration of the zwitterionic peptides while adding hydrophobic Leu groups in the sequence decreases the hydration of the peptide monolayer. The charge distribution in the peptide sequence is critical to the properties of surface tethered peptides. Our results quantitatively elucidate the effect of neutral spacer on the structure and properties of zwitterionic peptides, which, to our best knowledge, has not been systematically studied before. The current work provides useful molecular insights to the de novo design of functional zwitterionic peptides for a great realm of applications, such as coatings for medical equipment and implants[39, 40], drug delivery[41], and biosensors[42].

Experimental section

Materials. All the zwitterionic peptides with a purity of >95% were obtained from Genscript (Nanjing, China). The molecular weight (MW) of different sequences were characterized by MALDI-TOF (Autoflex tof/tofIII, Bruker, USA) as Figure S1. Tris(2-carboxyethyl)phosphine (TCEP), lysozyme, and bovine serum albumin were purchased from Sigma-Aldrich (Beijing, China). MilliQ water with a final resistivity 18 MΩ cm (Millipore

Milli-Q Plus, Millipore Corp., Bedford, MA) was used in all experiments.

X-ray photoelectron spectroscopy. We characterized the Au-peptide surfaces by X-ray photoelectron spectroscopy (XPS) (K-Alpha+ spectrometer, Thermo Fisher Scientific, UK). The high-resolution C(1s), N(1s), O(1s) and S(2p) spectra was collected a with a step size of 0.1 eV. The results were analyzed using Avantage software.

Preparation of zwitterionic peptide monolayer. The gold chip (BioNavis Ltd., Finland) was first cleaned in alkali piranha solution at 75 ℃ for 10 mins. After that, the chip was rinsed with ultrapure water followed by ultrasonic cleaner (KQ-250E, KunShan Ultrasonic Instruments Co., LTD, China). The chip was then dried with N_2 and then cleaned in an ultraviolet (UV)/ozone cleaning device for 1 h (PSD-UV4-Novascan, USA). Finally, the chip was rinsed with anhydrous ethanol and MilliQ water and dried with high-purity N_2. We dissolved zwitterionic peptide in PBS buffer (pH 7.4) with a final concentration of 1 mg/mL. TCEP solution was added into the peptide solutions with a molar ratio of 1:1 to break the disulfide bonds. The final concentration of the peptide was adjusted to 0.015 mM before the experiments.

Modification and nonspecific protein adsorption experiments. A SPR Navi 200A instrument (BioNavis Ltd., Finland) was used to measure the modification and the nonspecific adsorption of the foulants in real time. For each experiment, PBS buffer solution was flowed over the chip surface with a flow rate of 50 μL/min for approximately 10-20 min to establish the baseline. Then we injected the zwitterionic peptide solution at a flow rate of 5 μL/min for 40 min. Positively charged lysozyme and negatively charged BSA were selected as model

foulant to evaluate the antifouling performance. We dissolved lysozyme or BSA in PBS individually to the final concentrations of 1 mg/mL. Then we tested the antifouling performance by injecting the BSA or lysozyme solution at a flow rate of 10 μL/min for 10 min and rinsed with PBS buffer solution at a rate of 50 μL/min for 10 min. The shift in the SPR angle quantificationally indicate the amount of modification or foulants adsorption.[32, 35]

Morphology measured by AFM. We measured the morphology of modified surfaces in PBS buffer at room temperature by an AFM (Dimension Icon, Bruker) in ScanAsyst mode with a silicon AFM probe (SNL-10-C, Bruker, normal radius is 2 nm). Before the experiments, we rinsed the samples with MilliQ water and dried them with N_2. AFM images were processed using Gwyddion analysis software.

Static contact angle. The static contact angle was conducted using a OCA15EC device (DataPhysics Instruments, Germany). The data analysis was performed using the SCA 202 software. For each measurement, we deposited a 5 μL water droplet on the surfaces and measured the contact angle. The image was captured by a CCD camera, and the contact angle was determined by fitting the profile of the droplet. For each sample, the contact angle was averaged from 3 individual measurements.

Antibacterial tests. Fluorescent microscopy with 488 nm excitation light was used to test the anti-bacterial capability of the gold surface and peptide-modified gold surfaces against green fluorescent protein expressed E. coli. The bacteria were incubated in 10 mL LB Medium (with kanamicin) for 24 h at 37 °C under aerobic conditions and the bacteria density (10^7 CFU/mL) was determined using the spread plate method. The chips (bare gold and that

modified with peptides) were treated using 75% ethanol for sterilization before immersion into the bacteria solution. Afterwards, the chips were immersed into bacteria solution and incubated for 24 h, following rinsing by ultrapure water 3 times to remove the loosely-bound bacteria before the fluorescence test.

Surface force measurements. An SFA 2000 (SurForce LLC, Santa Barbara) was used for all the SFA measurements.[43] All peptides and protein solutions were prepared at concentrations of 0.015 mM and 1 mg/ml in PBS, respectively. The peptide and protein solutions were filtered using 0.22 μm nylon membrane. The procedure of the SFA experiments has been reported previously.[36] To graft the peptides onto the gold surface, freshly cleaved gold surface was immersed into 0.015 mM peptide solution for 12 h, followed by rinsing thoroughly with PBS buffer to remove the excess peptides, resulting in an uniform monolayers on (111) gold surfaces.[36, 44] Protein deposition was done by immersing the mica surface into a 1 mg/ml lysozyme solution for 15 min. After adsorption, the surfaces were gently rinsed to remove excess non-adsorbed protein from the surfaces. The SFA discs were then mounted in a SFA chamber and PBS was injected in between the surfaces prior to final equilibration. For each peptide-mica or peptide-protein experiments, the force runs (approach and separation cycles) were repeated 3 times for each condition.

Molecular dynamic simulations. We performed all-atom MD simulation with Amber_99SB-ILDN force field[45] and TIP3P water model by GROMACS 5.1.4.[37] For each simulation, 20 peptide chains were modified on the Au (111) surface and the volume of the box was 8.6 ×6.0 × 12.0 nm^3 (S/L) or 8.6 ×5.5 × 12.0 nm^3 (G) to resemble the modification density

of SPR experiments. To be consistent with experimental conditions, we added 137 mmol/L NaCl into the system to neutralize the charges. Periodic boundary conditions in the x- and y-directions were employed. Two repulsive LJ walls were included in the z-direction. Particle-mesh Ewald sum (PME) [46] method was used to evaluate the electrostatic interactions and the van der Waals interactions were calculated with energy and pressure corrections. 12 Å was used as the cut off. We minimized all these systems by steepest-decent minimization and heated the system to the target temperature of 298.15 K under canonical ensemble (NVT). The system was then equilibrated for 100 ns with a time step of 2 fs. The GROMACS inbuilt tools were used for data analysis, and the visual molecular dynamics (VMD) software was used to visualize the simulation results.[47]

Statistical analysis. We performed the statistical analysis (Table S1-S5) by student's t-test.[48]

ASSOCIATED CONTENT

Supporting Information

Supplementary Figures S1−S4 and Table S1-S6: Additional SPR data, AFM morphology, SFA force curve, MD simulation results and t-test analysis.

AUTHOR INFORMATION

Corresponding Authors

Rongxin Su - *State Key Laboratory of Chemical Engineering, Tianjin Key Laboratory of*

Membrane Science and Desalination Technology, Collaborative Innovation Center of Chemical Science and Engineering (Tianjin), School of Chemical Engineering and Technology, Tianjin University, Tianjin 300072, PR China; orcid.org/0000-0001-9778-9113; School of Marine Science and Technology, Tianjin University, Tianjin 300072, PR China; E-mail: surx@tju.edu.cn；

Jing Yu - *School of Materials Science and Engineering, Nanyang Technological University, 639798, Singapore*; orcid.org/0000-0002-4288-951X; E-mail: yujing@ntu.edu.sg;

Authors

Chuanxi Li - *State Key Laboratory of Chemical Engineering, Tianjin Key Laboratory of Membrane Science and Desalination Technology, Collaborative Innovation Center of Chemical Science and Engineering (Tianjin), School of Chemical Engineering and Technology, Tianjin University, Tianjin 300072, PR China;* orcid.org/0000-0003-2409-3347

Minglun Li - *School of Materials Science and Engineering, Nanyang Technological University, 639798, Singapore;* orcid.org/0000-0002-1286-6915

Wei Qi - *State Key Laboratory of Chemical Engineering, Tianjin Key Laboratory of Membrane Science and Desalination Technology, Collaborative Innovation Center of Chemical Science and Engineering (Tianjin), School of Chemical Engineering and Technology, Tianjin University, Tianjin 300072, PR China;* orcid.org/0000-0002-7378-1392

Complete contact information is available at https://pubs.acs.org/10.1021/xxx

Notes

The authors declare no competing financial interest.

ACKNOWLEDGEMENTS

CX L, and RX S acknowledge the National Natural Science Foundation of China (21621004), Tianjin Municipal Science and Technology Bureau, China (16JCZDJC37900), the Ministry of Education (grant No. NCET-11-0372), and the financial support from China Scholarship Council (CSC, 201806250100). M L and J Y thanks to Singapore Ministry of Education Academic Research Fund Tier 1 (RG7/19) and the Singapore National Research Fellowship (NRF-NRFF11-2019-0004).

References

1. Wu, J.; Han, H.; Jin, Q.; Li, Z.; Li, H.; Ji, J., Design and Proof of Programmed 5-Aminolevulinic Acid Prodrug Nanocarriers for Targeted Photodynamic Cancer Therapy. ACS Appl. Mater. Interfaces 2017, 9 (17), 14596-14605.

2. Lee, H.; Dellatore, S. M.; Miller, W. M.; Messersmith, P. B., Mussel-inspired Surface Chemistry for Multifunctional Coatings. Science 2007, 318 (5849), 426-30.

3. Wei, Q.; Becherer, T.; Angioletti-Uberti, S.; Dzubiella, J.; Wischke, C.; Neffe, A. T.; Lendlein, A.; Ballauff, M.; Haag, R., Protein Interactions with Polymer Coatings and Biomaterials. Angew. Chem. Int. Ed. Engl. 2014, 53 (31), 8004-31.

4. Bixler, G. D.; Bhushan, B., Biofouling: Lessons from Nature. Philos Trans A Math Phys Eng Sci 2012, 370 (1967), 2381-417.

5. Kim, S.; Gim, T.; Kang, S. M., Versatile, Tannic Acid-mediated Surface PEGylation for Marine Antifouling Applications. ACS Appl. Mater. Interfaces 2015, 7 (12), 6412-6.

6. Li, L.; Yan, B.; Yang, J.; Chen, L.; Zeng, H., Novel Mussel-inspired Injectable Self-healing Hydrogel with Anti-biofouling Property. Adv. Mater. 2015, 27 (7), 1294-9.

7. Xu, X.; Billing, M.; Ruths, M.; Klok, H. A.; Yu, J., Structure and Functionality of Polyelectrolyte Brushes: A Surface Force Perspective. Chem-Asian J 2018, 13 (22), 3411-3436.

8. Herrwerth, S.; Eck, W.; Reinhardt, S.; Grunze, M., Factors that determine the protein resistance of oligoether self-assembled monolayers - Internal hydrophilicity, terminal hydrophilicity, and lateral packing density. J. Am. Chem. Soc. 2003, 125 (31), 9359-9366.

9. Unsworth, L. D.; Sheardown, H.; Brash, J. L., Protein Resistance of Surfaces Prepared by Sorption of End-thiolated Poly(ethylene glycol) to Gold: Effect of Surface Chain Density. Langmuir 2005, 21 (3), 1036-41.

10. Arima, Y.; Toda, M.; Iwata, H., Complement Activation on Surfaces Modified with Ethylene Glycol Units. Biomaterials 2008, 29 (5), 551-60.

11. Greene, G. W.; Martin, L. L.; Tabor, R. F.; Michalczyk, A.; Ackland, L. M.; Horn, R., Lubricin: a Versatile, Biological Anti-adhesive with Properties Comparable to Polyethylene Glycol. Biomaterials 2015, 53, 127-36.

12. Ederth, T.; Lerm, M.; Orihuela, B.; Rittschof, D., Resistance of Zwitterionic Peptide Monolayers to Biofouling. Langmuir 2019, 35 (5), 1818-1827.

13. Jiang, S. Y.; Cao, Z. Q., Ultralow-Fouling, Functionalizable, and Hydrolyzable Zwitterionic Materials and Their Derivatives for Biological Applications. Adv. Mater. 2010, 22 (9), 920-932.

14. Blaszykowski, C.; Sheikh, S.; Thompson, M., Surface Chemistry to Minimize Fouling from Blood-based Fluids. Chem. Soc. Rev. 2012, 41 (17), 5599-612.

15. Yang, W.; Xue, H.; Carr, L. R.; Wang, J.; Jiang, S., Zwitterionic Poly(carboxybetaine) Hydrogels for Glucose Biosensors in Complex Media. Biosens. Bioelectron. 2011, 26 (5), 2454-9.

16. Cao, Z. Q.; Jiang, S. Y., Super-hydrophilic Zwitterionic Poly(carboxybetaine) and Amphiphilic Non-ionic Poly(ethylene glycol) for Stealth Nanoparticles. Nano Today 2012, 7 (5), 404-413.

17. Zhang, Z.; Chen, S.; Jiang, S., Dual-functional Biomimetic Materials: Nonfouling Poly(carboxybetaine) with Active Functional Groups for Protein Immobilization. Biomacromolecules 2006, 7 (12), 3311-5.

18. Mi, L.; Jiang, S., Integrated Antimicrobial and Nonfouling Zwitterionic Polymers. Angew. Chem. Int. Ed. Engl. 2014, 53 (7), 1746-54.

19. Zhao, C.; Zhao, J.; Li, X.; Wu, J.; Chen, S.; Chen, Q.; Wang, Q.; Gong, X.; Li, L.; Zheng, J., Probing Structure-antifouling Activity Relationships of Polyacrylamides and Polyacrylates. Biomaterials 2013, 34 (20), 4714-24.

20. Shao, Q.; Jiang, S., Molecular Understanding and Design of Zwitterionic Materials. Adv. Mater. 2015, 27 (1), 15-26.

21. Zhang, Z.; Chao, T.; Chen, S.; Jiang, S., Superlow Fouling Sulfobetaine and Carboxybetaine Polymers on Glass Slides. Langmuir 2006, 22 (24), 10072-10077.

22. Wang, G.; Han, R.; Su, X.; Li, Y.; Xu, G.; Luo, X., Zwitterionic Peptide Anchored to Conducting Polymer PEDOT for the Development of Antifouling and Ultrasensitive Electrochemical DNA Sensor. Biosens. Bioelectron. 2017, 92, 396-401.

23. Aili, D.; Stevens, M. M., Bioresponsive Peptide-Inorganic Hybrid Nanomaterials. Chem. Soc. Rev. 2010, 39 (9), 3358-70.

24. Ramakers, B. E.; van Hest, J. C.; Lowik, D. W., Molecular Tools for the Construction of Peptide-based Materials. Chem. Soc. Rev. 2014, 43 (8), 2743-56.

25. Wang, L.; Shi, C.; Wang, X.; Guo, D.; Duncan, T. M.; Luo, J., Zwitterionic Janus Dendrimer with distinct functional disparity for enhanced protein delivery. Biomaterials 2019, 215, 119233.

26. Wu, L. M.; Lin, B. Y.; Yang, H.; Chen, J.; Mao, Z. W.; Wang, W. L.; Gao, C. Y., Enzyme-responsive Multifunctional Peptide Coating of Gold Nanorods Improves Tumor Targeting and Photothermal Therapy Efficacy. Acta Biomaterialia 2019, 86, 363-372.

27. Khatayevich, D.; Gungormus, M.; Yazici, H.; So, C.; Cetinel, S.; Ma, H.; Jen, A.; Tamerler, C.; Sarikaya, M., Biofunctionalization of Materials for Implants Using Engineered Peptides. Acta Biomater. 2010, 6 (12), 4634-41.

28. Bolduc, O. R.; Pelletier, J. N.; Masson, J. F., SPR Biosensing in Crude Serum Using Ultralow Fouling Binary Patterned Peptide SAM. Anal. Chem. 2010, 82 (9), 3699-706.

29. Alvarez-Martos, I.; Moller, A.; Ferapontova, E. E., Dopamine Binding and Analysis in Undiluted Human Serum and Blood by the RNA-Aptamer Electrode. ACS Chem. Neurosci. 2019, 10 (3), 1706-1715.

30. Nowinski, A. K.; Sun, F.; White, A. D.; Keefe, A. J.; Jiang, S., Sequence, Structure, and Function of Peptide Self-assembled Monolayers. J. Am. Chem. Soc. 2012, 134 (13), 6000-5.

31. Chen, S.; Cao, Z.; Jiang, S., Ultra-low Fouling Peptide Surfaces Derived from Natural Amino Acids. Biomaterials 2009, 30 (29), 5892-6.

32. Li, C. X.; Liu, C. J.; Li, M. L.; Xu, X.; Li, S. Z.; Qi, W.; Su, R. X.; Yu, J., Structures and Antifouling Properties of Self-Assembled Zwitterionic Peptide Monolayers: Effects of Peptide Charge Distributions and Divalent Cations. Biomacromolecules 2020, 21 (6), 2087-2095.

33. Zhang, S.; Holmes, T.; Lockshin, C.; Rich, A., Spontaneous assembly of a self-complementary oligopeptide to form a stable macroscopic membrane. PNAS 1993, 90 (8), 3334-3338.

34. Smith, J.; McMullen, P.; Yuan, Z. F.; Pfaendtner, J.; Jiang, S. Y., Elucidating Molecular Design Principles for Charge-Alternating Peptides. Biomacromolecules 2020, 21 (2), 435-443.

35. Ye, H. J.; Xia, Y. Q.; Liu, Z. Q.; Huang, R. L.; Su, R. X.; Qi, W.; Wang, L. B.; He, Z. M., Dopamine-assisted deposition and zwitteration of hyaluronic acid for the nanoscale fabrication of low-fouling surfaces. J. Mater. Chem. B 2016, 4 (23), 4084-4091.

36. Yu, J.; Kan, Y. J.; Rapp, M.; Danner, E.; Wei, W.; Das, S.; Miller, D. R.; Chen, Y. F.; Waite, J. H.; Israelachvili, J. N., Adaptive hydrophobic and hydrophilic interactions of mussel foot proteins with organic thin films. PNAS 2013, 110 (39), 15680-15685.

37. Pronk, S.; Pall, S.; Schulz, R.; Larsson, P.; Bjelkmar, P.; Apostolov, R.; Shirts, M. R.; Smith, J. C.; Kasson, P. M.; van der Spoel, D.; Hess, B.; Lindahl, E., GROMACS 4.5: a High-throughput and Highly Parallel Open Source Molecular Simulation Toolkit. Bioinformatics 2013, 29 (7), 845-54.

38. Zhang, L. Y.; Wang, L. J.; Kao, Y. T.; Qiu, W. H.; Yang, Y.; Okobiah, O.; Zhong, D. P., Mapping hydration dynamics around a protein surface. PNAS 2007, 104 (47), 18461-18466.

39. Pavithra, D.; Doble, M., Biofilm Formation, Bacterial Adhesion and Host Response on Polymeric Implants-issues and Prevention. Biomed. Mater. 2008, 3 (3), 034003.

40. Chang, J.; Tao, Y.; Wang, B.; Guo, B. H.; Xu, H.; Jiang, Y. R.; Huang, Y. B., An in Situ-forming Zwitterionic Hydrogel as Vitreous Substitute. J. Mater. Chem. B 2015, 3 (6), 1097-1105.

41. Jin, Q.; Deng, Y.; Chen, X.; Ji, J., Rational Design of Cancer Nanomedicine for Simultaneous Stealth Surface and Enhanced Cellular Uptake. ACS Nano 2019, 13 (2), 954-977.

42. Sabaté del Río, J.; Henry, O. Y. F.; Jolly, P.; Ingber, D. E., An Antifouling Coating that Enables Affinity-based Electrochemical Biosensing in Complex Biological Fluids. Nat. Nanotech. 2019, 14 (12), 1143-1149.

43. Israelachvili, J.; Min, Y.; Akbulut, M.; Alig, A.; Carver, G.; Greene, W.; Kristiansen, K.; Meyer, E.; Pesika, N.; Rosenberg, K.; Zeng, H., Recent advances in the surface forces apparatus (SFA) technique. Rep Prog Phys 2010, 73 (3).

44. Valtiner, M.; Donaldson, S. H.; Gebbie, M. A.; Israelachvili, J. N., Hydrophobic Forces, Electrostatic Steering, and Acid-Base Bridging between Atomically Smooth Self-Assembled Monolayers and End-Functionalized PEGolated Lipid Bilayers. J. Am. Chem. Soc. 2012, 134 (3), 1746-1753.

45. Lindorff-Larsen, K.; Piana, S.; Palmo, K.; Maragakis, P.; Klepeis, J. L.; Dror, R. O.; Shaw, D. E.,

Improved Side-chain Torsion Potentials for the Amber ff99SB Protein Force Field. Proteins 2010, 78 (8), 1950-8.

46. Darden, T.; York, D.; Pedersen, L., Particle mesh Ewald: An N · log (N) method for Ewald sums in large systems. J. Chem. Phys. 1993, 98 (12), 10089-10092.

47. Humphrey, W.; Dalke, A.; Schulten, K., VMD: Visual Molecular Dynamics. J Mol Graph 1996, 14 (1), 33-8, 27-8.

48. Kalpić, D.; Hlupić, N.; Lovrić, M., Student's t-Tests. In International Encyclopedia of Statistical Science, Lovric, M., Ed. Springer Berlin Heidelberg: Berlin, Heidelberg, 2011; pp 1559-1563.

For Table of Contents Use Only